Copper-doped tin oxides supported on mesoporous carbon xerogel for boosting the electrochemical reduction of CO_2 to formate in bicarbonate solution coupled with CO_2

Pom L. Kharel[1], Muthu K. Gnanamani[2], Md Ariful Hoque[2], Keemia Abad[1,3], Neng Huang[1,4], Xin Gao[1,4], Kunlei Liu[1,4], Ayokunle O. Omosebi[1], and Jesse Thompson[,1,3]*

[1]University of Kentucky Institute for Decarbonization and Energy Advancement, Lexington, Kentucky 40506, United States

[2]University of Kentucky Center for Applied Energy Research, Lexington, Kentucky 40511, United States

[3]Department of Chemistry, University of Kentucky, Lexington, Kentucky 40506, United States

[4]Department of Mechanical and Aerospace Engineering, University of Kentucky, Lexington, Kentucky 40506, United States

*Corresponding author

Jesse Thompson: jesse.thompson@uky.edu

Keywords: Electrocatalytic reduction, formic acid, carbon xerogel, bipolar membrane, bimetallic electrocatalyst

Abstract

The electrochemical reduction of CO_2 into valuable products at mild reaction conditions and using cheap renewable electrical energy is a goal to sustain a low-carbon economy. Among the various CO_2 reduction reaction products, formic acid (FA) has received significant attention because of its low Gibbs free energy input requirement and the simple reduction reaction involving the transfer of 2 electrons and 2 protons. In this work, a copper-doped tin oxide catalyst supported on mesoporous carbon xerogel was shown to enhance the electrochemical reduction of CO_2 to formate in a bicarbonate solution coupled with CO_2. We observed that the synergistic SnCu oxides enhance the selectivity towards formate from 58.6% for Sn oxide and 28.7% for Cu oxide to over 71.2% for the SnCu oxides. The observed rate of formate production with SnCu oxide was 2.8 times higher compared to the rate of Cu oxide, and about 1.5 times higher than the Sn oxide catalyst. Our results reveal that selectivity for formate comes partly from the electrolysis of bicarbonate solution and partly from continuous CO_2 gas purged into solution. The contribution from the electrolysis of bicarbonate solution ranges from 15% to 40% when the concentration of bicarbonate solution ranges from 100 mM to 1 M. Chronoamperometric measurements for stability revealed that Cu oxide and Sn oxide showed stable current density for less than 30 h while under the same conditions, the stable current density was observed for more than 50 h with SnCu oxide catalyst. Additionally, the selectivity towards formate increased by 6% when the reactor pressure was increased from near ambient pressure to 4 psig. Our lab-scale electrochemical cell with SnCu oxide supported on the mesoporous carbon xerogel enhances the CO_2 solubility, minimizes the precipitation of salts that can degrade the catalytic performance, and suppresses the competitive hydrogen evolution reaction, demonstrating the feasibility of using our catalyst and system for the electrochemical conversion of CO_2 into formate with high selectivity, productivity, and stability. This could have significant implications for the mitigation of CO_2 emissions and the development of sustainable chemical industry.

1 **Graphical abstract**

2 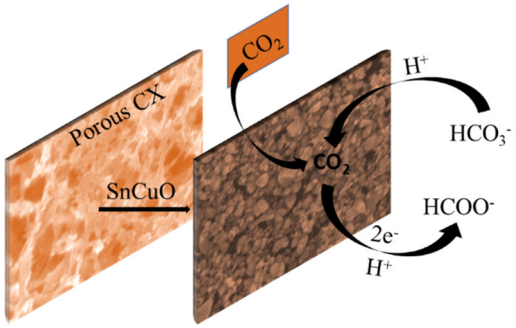

3

4

1. Introduction

The concentration of atmospheric CO_2 gas is increasing past 420 ppm, 50% higher than pre-industrial levels.[1] The consequence of this can influence climate change, as well as air quality and energy security.[2] Carbon capture, utilization, and sequestration are regarded as crucial strategies for mitigating the problems arising from increasing CO_2 concentration in the atmosphere. Carbon utilization through photocatalysis,[3] electrocatalysis, hydrothermal conversion[4, 5] and biological transformation[6] is an appealing route for reducing CO_2 to produce value-added chemicals like methane, ethane, ethylene, formic acid, and large +C2 products. Electrochemical reduction of CO_2 can be performed at mild reaction conditions and can use cheap renewable electrical energy without any additional fossil fuel-based electric power sources,[7] to obtain a wide selection of products.[8, 9]. Electrochemical reduction of CO_2 involves generating the anion radical ($CO_2^{\cdot-}$), which is formed when the CO_2 molecule gets sufficient energy and is adsorbed on the catalyst surface.[10] The different reaction pathways involved in the electron-proton transfer steps can lead to a wide distribution of CO_2 reduction reaction (CO_2RR) products. The CO_2RR products are determined by many process variables such as the catalyst (type and morphology), temperature, pressure, reduction potential, electrolyte (type, concentration and pH), solvent (aqueous or nonaqueous), membrane separator, design of electrochemical reactor, etc.[11-17] A key challenge is developing electrocatalysts tuned to produce the desired product with high selectivity and productivity while working best in a wide range of potentials in competition with the hydrogen evolution reaction (HER)[18] and whilst remaining stable in the reaction conditions.

Electrocatalysts undertake the most prominent role in determining the reaction pathway, thereby enabling CO_2RR with high activity and selectivity. Metals are the most investigated catalysts for CO_2RR. The metals which catalyze CO_2RR can generally be (i) formate/formic acid (FA) selective (Pb, Hg, In, Sn, Bi, Cd, Ti), (ii) CO selective (Au, Ag, Zn, Pd, Ga), (iii) H_2 selective (Pt, Ni, Fe, Ti) or (iv) hydrocarbon selective (Cu and Cu-based catalysts).[19, 20] Compared to elemental metals, metal oxides are shown to have more active sites, and are widely investigated for their catalytic activity for CO_2 reductions.[21, 22] Many reports reveal that the metal oxides with oxygen deficiency provide and stabilize highly active sites for CO_2 activation, thereby enhancing electrocatalytic performance with lower overpotential.[23-25] Among the various CO_2RR products, CO and FA have received a significant attention because of their low Gibbs energy input

requirement and the reduction reaction involving the simple transfer of 2 electrons and 2 protons. CO_2 reduction to FA is favored most thermodynamically as the standard free energy of formation of FA -361.4 kJ/mol is very close to that of CO_2 -394.4 kJ/mol and needs the lowest Gibbs energy input. Moreover, FA is a liquid state at room temperature and atmospheric pressure and is easier to store and handle than gaseous products. Currently, FA is widely used as a preservative and an antibacterial agent in livestock feeds, as well as for leather tanning, and in rubber industries.[26-28] The potential future markets of FA include direct formic acid fuel cells and as a liquid H_2 storage medium.[29-31]

Numerous electrocatalysts including Bi and Bi oxides,[22, 32-34] Sn and Sn-based electrocatalysts,[35-38] enzymes,[16] and nano In/Ag composite[39] are studied for the electrochemical conversion of CO_2 to formate/FA. Sn and Sn-based catalysts are well focused materials for they are cost effective and eco-friendly. The gas diffusion electrodes of these catalysts with different electrolytes, membranes and cell configurations have shown to perform with high FE and current densities for formate/FA.[40-42] Although Cu and Cu-based catalysts are associated with hydrocarbon selectivity,[19, 20] recent studies reveal that nano Cu and Cu oxides are capable of reducing CO_2 to formate/FA with exceptionally high selectivity.[43, 44] However, many of these investigations have been limited in duration, with catalyst performance showing signs of decline over time. One strategy to enhance catalyst properties is to the utilization of synergetic metals. Synergistic bimetallic electrocatalysts can have a promising avenue for improving activity and selectivity compared to their monometallic counterparts by fine-tuning their structure, morphology, and composition.[45-47] Bimetallic electrocatalysts, such as In-Bi,[48] Zn-Bi,[49] Sn-Cu,[50] Bi-Eu,[51] Pd-Bi,[52] Bi-Sb,[53] Sn-In,[54] and Sn-Zn,[55] have demonstrated to promote the conversion of CO_2 to formate/FA. Recently, Liu et al. reported bimetallic Sn-Cu electrocatalyst showing over 80% FE, however, the performance was limited to 20h and higher overpotential (-1.11 V vs. RHE).[56] Most of these studies use flow through reactors under high pressure. The narrow potential window for formate/formic production, high overpotential, long-term stability issues arising from electrolyte precipitation and catalyst transformation, complex and costly procedure for catalyst synthesis are the chief shortcomings.

In this work, we investigate bimetallic SnCu oxides synthesized by wet chemistry that are not only capable suppressing the hydrogen evolution reaction but also effectively promoting the

reduction of CO_2 to formate/FA. Doping Cu to Sn oxide is explored to increase the selectivity for formate production with a wider potential window, reduced overpotential, and improved stability. Since formate can be formed by the direct reduction of CO_2 that is dissolved in water or CO_2 generated in situ by the reaction of protons with bicarbonate, increasing the reactor pressure was explored to boost dissolved CO_2 and formate production. In addition, the faradaic efficiency for formate was explored with the best performing SnCu oxide and potassium bicarbonate solution only, without purging any CO_2, wherein the efficiency dependence on the concentration of potassium bicarbonate will be examined. Furthermore, the effect of bicarbonate concentration on electrolyte precipitation on the electrode surface is explored, including the consequential impact on electrocatalytic performance and stability.

2. Experiments and Methods

2.1 Chemicals. Fumasep FBM (bipolar membrane), plain carbon cloth (code 1592020), CeTech carbon cloth, and alcohol-based Nafion dispersion (5% w/w) were purchased from FuelCellStore, USA. Potassium carbonate (ACS grade, 99.7%), potassium bicarbonate (ACS grade, >99.0%), sulphuric acid (96%), anhydrous sodium carbonate (99.9%), resorcinol (≥99.0%), ethanol (ACS reagent, ≥99.5%), isopropanol (ACS reagent, ≥99.5%), copper nitrate ($Cu(NO_3)_2.2.5H_2O$, 99.99%), and acetone were purchased from Sigma Aldrich, USA. Tin (II) chloride ($SnCl_2.2H_2O$, 99%) was obtained from Fisher Science Education, USA. Concentrated ammonium hydroxide (ACS reagent grade, 29%) was purchased from VWR chemicals, USA.

2.2 Synthesis of carbon xerogel on carbon cloth. Mesoporous carbon xerogel was developed on commercial carbon cloth (Fuel Cell Store) by polycondensation of resorcinol and formaldehyde in a basic medium reported in the literature.[57] Briefly, 10.0 g of resorcinol, 14.7 g of 37% w/w formaldehyde, 10.9 g of deionized water and 3.00 g of 20 mM sodium carbonate were mixed, and the mixture was magnetically stirred for 15 min at 125 RPM to get a clear solution. The clear solution was spread on a commercial carbon cloth and sandwiched between glass plates with no air bubbles trapped. The glass plates were tightly held with binder clips and duct tape, wrapped with aluminum foil, and heated in an oven at 100°C for 30 h. The duct tape was carefully removed, and the carbon cloth was soaked for 2 h each, first in deionized water, followed by in acetone. The substrate was then heated and cooled in a furnace in a nitrogen atmosphere with the temperature ramp shown in Figure S1 (Supplementary Information).

2.3 Synthesis of Sn and SnCu oxides. The Sn and SnCu oxides were synthesized using a two-step wet-chemistry method published elsewhere.[58] The first step involves the precipitation of metal oxyhydroxide, and the subsequent step involves thermal transformation of metal oxyhydroxide to metal oxide.

(a) For Sn oxide, 0.02 moles of tin chloride ($SnCl_2.2H_2O$) was dissolved in 200 mL of ice-cold deionized water in a 250 mL round-bottom flask. The solution was stirred with nitrogen purging for an hour. The temperature of the round bottom flask must be maintained in a range of 5-10 ℃ to avoid Sn^{2+} oxidation triggered at room temperature. At this point, the solution turns milky white with a pH around 2. Following this, 5.6 mL of concentrated ammonium hydroxide (0.04 moles) was added dropwise to the metal solution. The mixture was stirred for about an hour. Finally, the precipitate was filtered and washed with copious amounts of deionized water followed by anhydrous ethanol (Aqua Solutions MS denatured, anhydrous USA). The sample was dried in a vacuum desiccator at room temperature for 24 h. In the second stage, 1 gram of dry sample obtained from the above process was dispersed in 100 mL of ethanol-water mixture 70:30 (v/v) and refluxed overnight at 80 ℃. The resultant slurry solution was filtered and washed with anhydrous ethanol to dry.

(b) For SnCu oxide of a desired composition, an appropriate amount of copper nitrate ($Cu(NO_3)_2.2.5H_2O$, 99.99% Aldrich, USA) was dissolved in 50 mL of ice-cold deionized water. This solution was added to 150 mL of a solution containing an appropriate amount of tin chloride ($SnCl_2.2H_2O$) so that the stoichiometric ratio of Sn and Cu in the catalyst was defined by the molar ratio of Sn and Cu salts. The content in the flask was stirred continuously at the temperature 5-10 ℃ for an hour before the precipitant, ammonium hydroxide, was added. Finally, the precipitate was filtered and washed with copious amounts of deionized water followed by anhydrous ethanol. The precipitate was dried in a vacuum desiccator at room temperature for 24 h. 1 gram of the dry sample so obtained was dispersed in 100 mL of ethanol-water mixture 70:30 by volume and refluxed overnight at 80 ℃. The resultant slurry solution was filtered and washed with anhydrous ethanol to dry.

2.4 Catalyst coating. A spray-coating method by an airbrush (Master Airbrush, 0.2 mm nozzle) was used to make the working electrode for all the catalyst coated electrodes reported here. First, the ink solution was prepared by sonicating a mixture of catalyst, activated carbon, Nafion

dispersion, deionized water, and isopropanol. Subsequently, the ink was spray-coated on the substrate. CeTech carbon cloth was used as a substrate for cyclic voltammetry and electrochemical impedance spectroscopy, while CX was used for all other experiments. The mass of catalyst loaded, calculated as the mass difference of the substrate before and after coating catalyst, divided by its geometric area gives the catalyst loading. The catalyst loadings for different electrodes are summarized in Table 1.

Table 1. Catalyst loading (CL) of electrodes

Substrate	Catalyst	Name of electrode	CL (mg/cm^2)	Reference to
CX	CuO	CX_CuO	1.75	Fig. 2a, 4a
CX	SnO	CX_SnO	1.16	Fig. 2b, 4b
CX	$Sn_{70}Cu_{30}$	CX_$Sn_{70}Cu_{30}$	1.56	Fig. 2c, 4c
CX	$Sn_{95}Cu_5$	CX_$Sn_{95}Cu_5$	1.09	Fig. 2d, 4d
			1.43	Fig. 6a-e
			1.52	Fig. 8a-d
CeTech CC	$Sn_{95}Cu_5$	CT_$Sn_{95}Cu_5$	0.86	Fig. 7a-c

2.5 Electrochemical measurement. Electrochemical measurements were carried out in an H-cell using aqueous $KHCO_3$ as a catholyte, H_2SO_4 as an anolyte, separated by a Fumasep bipolar membrane as a membrane with the cation exchange facing towards cathode. A reverse bias mode BPM facilitates water-splitting by generating protons that diffuse to the cathodic chamber through its cation exchange layer. Typically, alkaline solutions are utilized as anolytes with bicarbonate catholyte solutions to mitigate potential losses stemming from pH variations.[59] Research has indicated that in an alkaline anolyte, the anion exchange layer of the BPM deteriorates over time, leading to increased resistance in water-splitting,[60] however, some commercial BPMs may have extra stability over large pH range. Although employing an acid as an anolyte with a BPM may lead to potential losses and could necessitate the use of a previous metal for the anode, the stability

of the BPM's anion exchange layer benefits from contact with acid. The H_2SO_4 concentration was 0.4 M, while $KHCO_3$ concentration ranged from 0.1 to 1.0 M. Our electrochemical cell uses a leak-free Ag/AgCl, 3.5 M NaCl electrode as a reference electrode, the electrode coated with a catalyst as a working electrode and platinum mesh as a counter electrode. Moist CO_2 gas was bubbled into the catholyte at 10 mL/min through a sparger. Figure 1 depicts the general scheme of the experimental setup for the electrochemical measurements. The actual digital picture of the electrochemical cell can be found in Figure S2 (Supplementary Information).

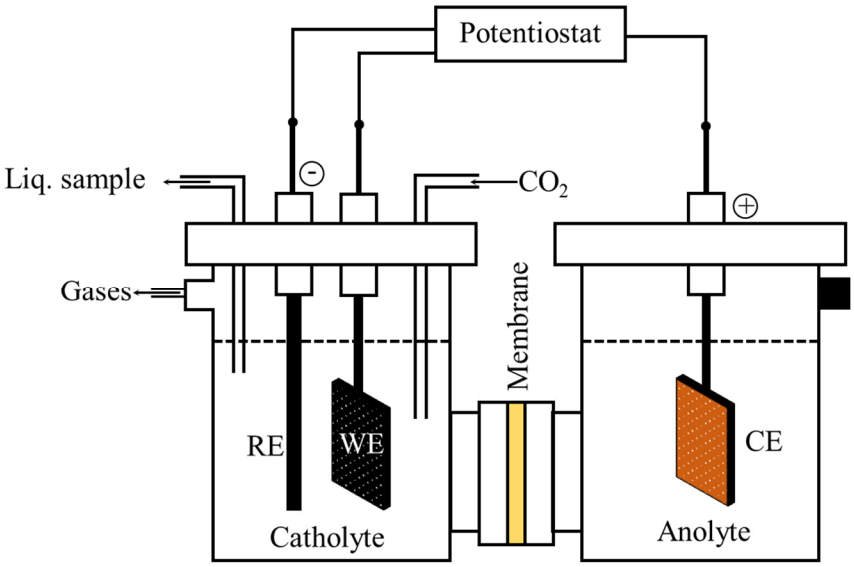

Figure 1. Scheme of the experimental setup for electrochemical measurement for CO_2RR. Herein, working electrode (WE) is the catalyst-coated electrode, counter electrode (CE) is a Pt mesh, and reference electrode is a leak free Ag/AgCl, 3.5 M NaCl.

Prior to any electrochemical measurement, dry N_2 gas was purged into the catholyte solution for 15 min to remove dissolved O_2. Following this, moist CO_2 gas was bubbled into the catholyte solution at the rate 10 mL/min for 15 minutes. Three types of electrochemical measurements, namely chronoamperometry, cyclic voltammetry (CV) and electrochemical impedance spectroscopy (EIS) were performed with Biologic SP-200 potentiostat. For chronoamperometric measurement, a desired reduction potential was applied to the working electrode (WE) and the electric current (i) was measured as a function of time (t). The WEs are denoted as CX_catalyst hereafter. For example, CX coated with tin oxide will be named as CX_SnO. The total charge (Q)

used for the calculation of catalytic performance was obtained by integrating the current (i) with time (t), as shown below:

$$Q = \int_0^t idt \ldots (i)$$

For CV and EIS measurements, CeTech carbon cloth (CT) was used as a substrate, thereby avoiding the substantial capacitive contributions of CX on the V-i measurements. The WEs prepared on CeTech carbon cloth are denoted by CT_catalyst hereafter. CV measurements were carried out in a dilute $KHCO_3$ solution for at least 5 cycles.

2.6 Evaluation of catalytic performance. Catalytic performance for CO_2RR to formate was evaluated based on the faradaic efficiency (FE) calculated as

$$\mathrm{FE} = \frac{2 \times 96485 \left(\frac{\mathrm{C}}{\mathrm{mol}}\right) \times \mathrm{N_{formate}\ (mol)}}{\mathrm{Q_T}} \times 100\% \ldots (\mathrm{ii})$$

where $N_{formate}$ is the number of moles of formate produced when a total charge of Q_T is passed through the cell. Formate detection and quantification were performed with a Dionex ICS-6000 Ion Chromatography system (Dionex-ThermoScientific, Sunnyvale, CA) and an AS autosampler. The anion system consisted of an ADRS 600 suppressor, an EGC 500 KOH eluent generator, an IonPac AS15 analytical column and an AG15 guard. Formate was eluted using an isocratic KOH concentration of 15 mM for 12 minutes. A certified standard of formate was obtained at a stock concentration level of 100 mg/L from Environmental Express (Charleston, SC). Individual calibration standards were prepared by diluting the stock solutions with 18.2 MΩ water. The samples were diluted prior to IC analysis with each sample analyzed in triplicate. Peak identification and integration were performed manually using Dionex Chromeleon chromatography management system software version 7. The concentration of formate ($C_{formate}$) in the liquid phase was quantified using a calibration curve established by the standard formate anion and the calibration curve was used to calculate $N_{formate}$ as follows:

$$N_{formate} = C_{formate}\ (M) \times V_{ele}\ (L) \ldots (iii)$$

where V_{ele} is the volume of the electrolyte used during the electrochemical measurement (100 mL in our case). The potential of the working electrode was controlled with the leak-free Ag/AgCl,

3.5 M NaCl as a reference electrode, and expressed relative to the reversible hydrogen electrode by using $E_{RHE} = E_{Ag/AgCl} + 0.209\ V + 0.059 \times pH$.[61] Furthermore, the rate of formate production $rate_{formate}$ was derived from $N_{formate}$, normalized by time (t) for which the reduction was carried out, and geometric area (A) of the electrode immersed in the solution as:

$$rate_{formate} = \frac{N_{formate}}{t \times A} \ldots (iv)$$

3. Results and Discussions

Carbon xerogel synthesized on commercial carbon is mesoporous compared to macroporous commercial carbon (Figures S3, Supplementary Information). The solid-state electrical conductivity measurement using the four-probe method (Figure S4, Supplementary Information) reveals that the electrical conductivity of CX is about 80% of that plain carbon cloth (Figures S5, Supplementary Information). However, CX is better at accommodating a sufficient catalyst loading, which is essential for the electrochemical measurement and prevention of catalyst leaching. SEM images of different catalysts coated on CX by airbrushing are shown in Figure 2. SEM images of SnCu oxide particles airbrushed on CX are depicted in Figure 2c-d. The EDS spectra shown in Figures S6 and S7 (Supplementary Information) reveal that the synthesized these particles in Figures 2c and 2d had about 73 mol% and 96 mol% of Sn respectively. These electrodes are referred to as CX_CuO, CX_SnO, CX_$Sn_{70}Cu_{30}$ and CX_$Sn_{95}Cu_5$ hereafter.

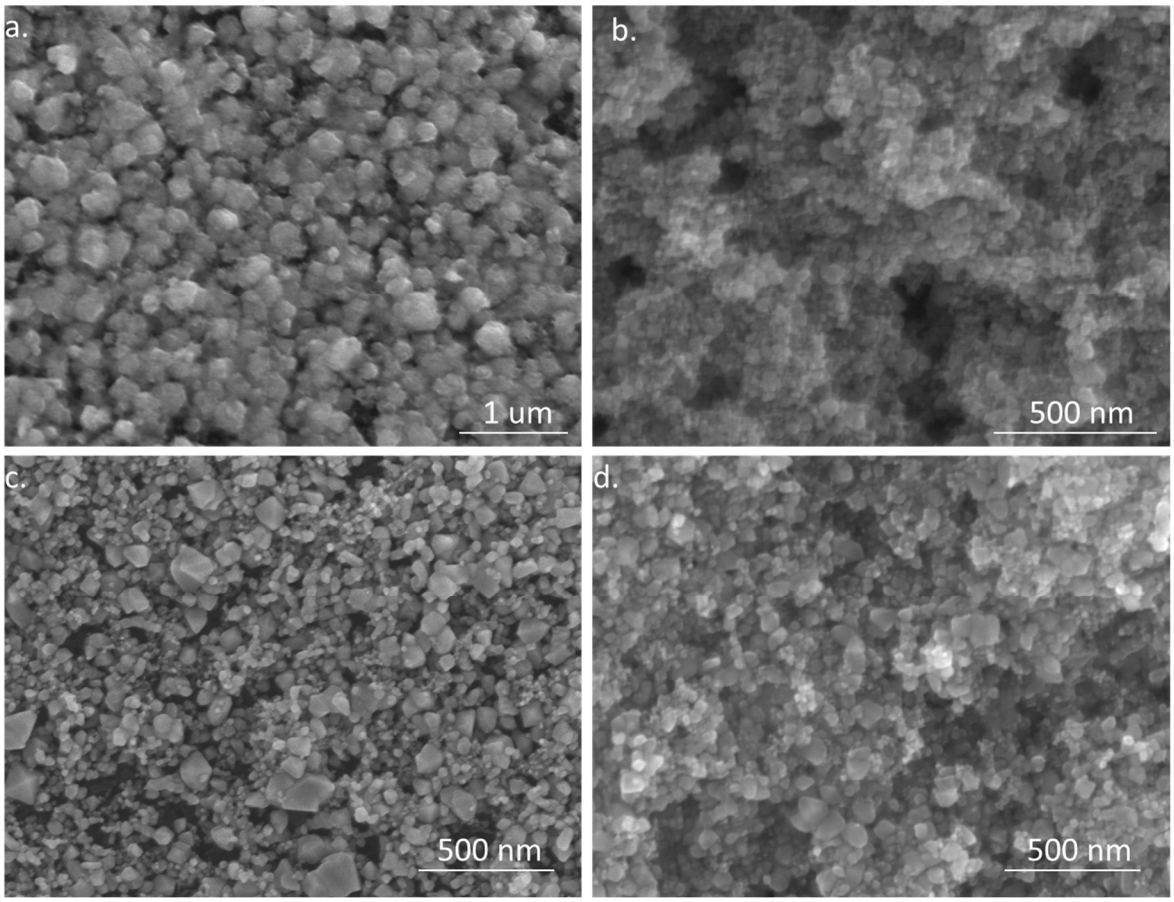

Figure 2. SEM images of catalyst-coated electrodes (a) CX_CuO, (b) CX_SnO, (c) CX_$Sn_{70}Cu_{30}$, and (d) CX_$Sn_{95}Cu_5$.

The prepared catalyst particles were further characterized by X-ray diffraction (XRD) spectroscopy. The p-XRD spectra of SnCu oxides with 100, 95 and 70 mol% of Sn are shown in Figure 3. The XRD spectra of Sn oxide particles show both Sn (II) and Sn (IV) oxides. The peaks marked by ■, # and Δ correspond to Sn (II), Sn (IV) and both Sn (II) and Sn (IV) oxides respectively, consistent with the literature.[62-64] The spectra of $Sn_{95}Cu_5$ were identical to the spectra of SnO except for the peak at $2\theta = 51.4°$ and bump around $2\theta = 65°$. These features became more distinct as the mol% of Cu was increased to 30. These features correspond to SnCu oxide only.[65] Interestingly, the peak positions of SnO at lower 2θ were found to be shifted to a higher angle with Cu-doping. This indicates that Cu-doping has changed the lattice parameters. There were no features corresponding to Cu_2O and CuO particles in the SnCu oxides (Figure S8, Supplementary Information), indicating no/insignificant discrete Cu oxide particles.

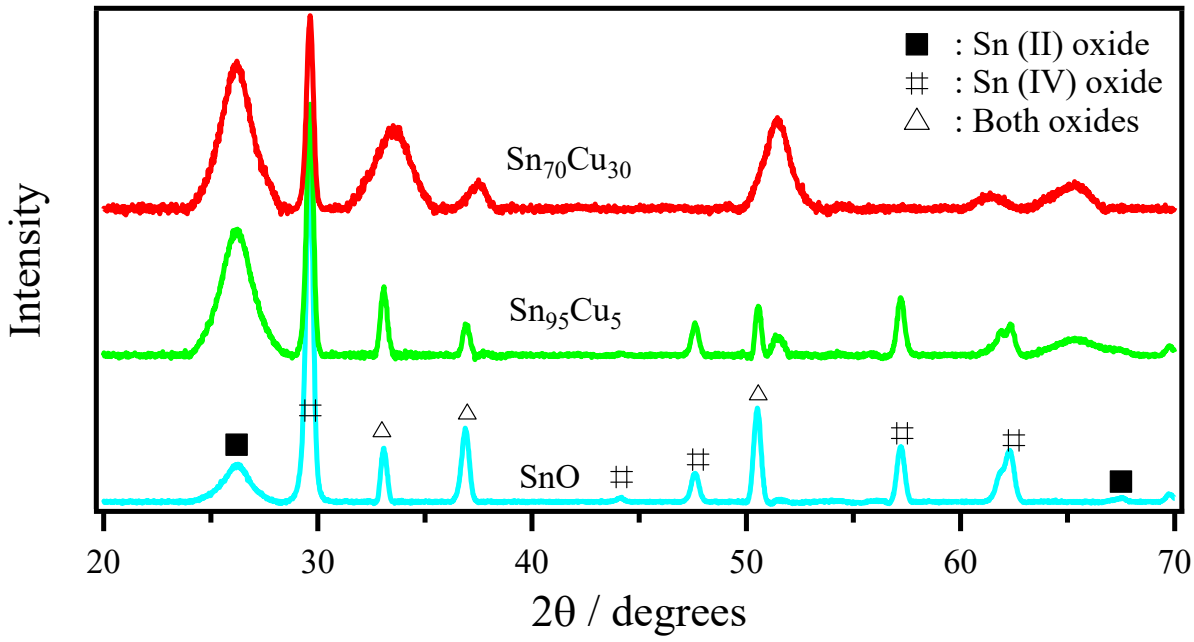

Figure 3. p-XRD patterns of as-prepared SnCu oxides with 100, 95 and 70 mol% of Sn.

The electrochemical reduction of CO_2 to formate was evaluated using CX_SnO, CX_CuO, CX_$Sn_{70}Cu_{30}$ and CX_$Sn_{95}Cu_5$ as working electrodes in a 1 M potassium bicarbonate solution by applying reduction potentials from -0.5 V to -1.1 V vs. RHE. Chronoamperometric experiments were run for at least 3 h at each potential using the different electrodes of comparable areas, and fresh electrolyte. The current density (j) and FE for formate involved in the electrochemical conversion of CO_2 for each of these electrodes are depicted in Figure 4. For CX_CuO, the j increases gradually with the increase of the reduction potential from -0.60 V through -0.85 V vs. RHE (Figure 4a). Starting with FE of 7.3% at -0.60 V vs. RHE, the selectivity of formate increased to 28% at -0.85 V vs. RHE (cell potential: 4.2 V). These results are better than literature in terms of both energy consumed and selectivity towards formate.[66] After -0.85 V vs. RHE, there is a sharp increase in the j, but the FE for formate is found to drop drastically, indicating that there is another Faradaic process occurring predominantly after that potential, presumably hydrogen evolution reaction or CO_2 reduction to other products. The catalytic performance of tin oxide (CX_SnO) in 1 M potassium bicarbonate is depicted in Figure 4b. The production of formate was insignificant at more positive potentials than -0.60 V vs. RHE. The selectivity for FA increased at potentials more negative to -0.65 V through -0.85 V vs. RHE. The maximum FE of 59.2% was observed at -0.74 V vs. RHE (cell potential: 3.4 V), and the corresponding j was 11.2 mA cm^{-2} consistent with

the performance of SnO nanowires.[67] As in the experiments with CX_CuO, the j started to increase sharply after -0.85 V vs RHE, while FE decreased indicating occurrence of other Faradaic processes. Notably, the overpotential for FA production with CX_SnO was found to be about 150 mV less than with CX_CuO. These results are also consistent with the reports which reveal that Sn and Sn-based catalysts are more selective for FA.[68-70] When copper-doped SnO was used as the WE, the selectivity for formate was further improved. Figure 4c shows the j and FE for formate of the CCE CX_$Sn_{70}Cu_{30}$ at different reduction potentials ranging from -0.6 V to -1.05 V vs. RHE in 1 M potassium bicarbonate solution. Similar to the results of CX_SnO, FA production started to increase above -0.65 V vs. RHE. A maximum FE above 70% was observed at -0.74 V vs. RHE (cell potential: 3.3 V), corresponding to the optimum performance. A sharp increase in the j at the potential more negative to -0.85 V vs. RHE, accompanied by a reduction in FE, indicates the occurrence of other Faradaic processes. The selectivity for formate remained above 60% for the potential range -0.70 V through -0.90 V vs. RHE. Consistent results were obtained with CX_$Sn_{95}Cu_5$ (Figure 4d), but at slightly lower reduction potential of -0.72 V vs. RHE (cell potential: 3.2 V). It is very interesting to note here that the reduction potential for CO_2 to formate shifted towards a more positive potential as the mol% of Cu goes lower. For instance, at -0.65 V vs. RHE, FE for formate was ~10% with CX_SnO and CX_Cu, ~ 20% CX_$Sn_{70}Cu_{30}$, while it was ~40% for CX_$Sn_{95}Cu_5$. Cu doping in SnO is found to decrease overpotential and increase the potential range for which CO_2 gets reduced to FA. Compared to CX_$Sn_{70}Cu_{30}$, CX_$Sn_{95}Cu_5$ had a narrower potential window (-0.69 V to -0.74 V vs. RHE) for formate production.

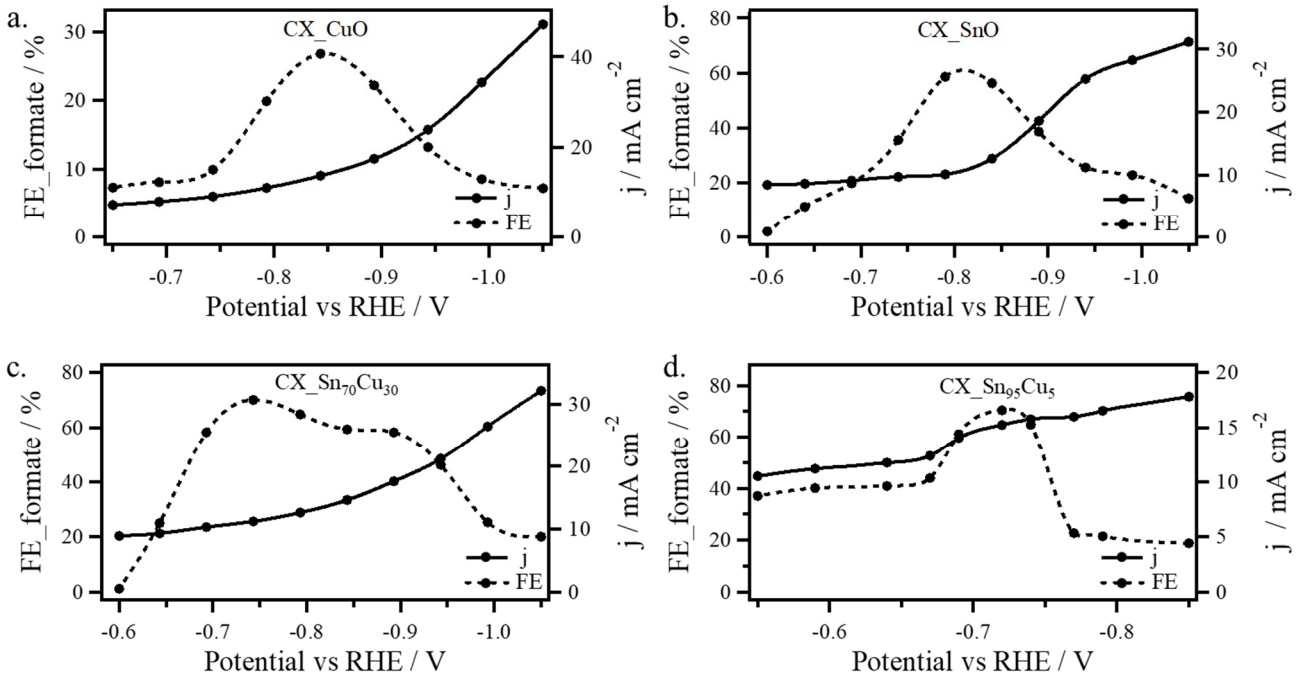

Figure 4. The j and the FE for formate production involved in the electrochemical reduction of CO_2 at different reduction potentials ranging from -0.6 V through -1.1 V vs. RHE: (a) CX_CuO, (b) CX_SnO, (c) CX_$Sn_{70}Cu_{30}$ and (d) CX_$Sn_{95}Cu_5$. Chronoamperometric/coulometric curves for these catalyst-coated electrodes (CCE) at the potential where formate was produced significantly can be found in Figure S9 (Supplementary Information).

The data from Figure 4 were used to calculate the rate of production of formate. The rates were normalized with the geometric area of the electrode and experiment run time as described in the section 2.6 (equation (iv). In general, the rate of production of formate followed the same trend as the FE, especially more positive to -0.85 V vs. RHE. For the reduction potential more negative to -0.85 V vs. RHE, the rate increased or decreased based on the charge passed and the catalyst itself. For the WE CX_CuO, the j increased sharply after -0.85 V, due to which more charge was passed, and the rate of production of formate was 71.6 μmol h^{-1} cm^{-2} at -0.89 V vs. RHE, and it remained above 50 μmol $h^{-1}cm^{-2}$ for the potential range -0.80 V through -1.05 V vs. RHE (Figure 5a). In the case of CX_SnO, the maximum formate production of 132.6 μmol h^{-1} cm^{-2} was observed at -0.89 V vs. RHE, and it remained above 100 μmol $h^{-1}cm^{-2}$ for the potential window -0.79 V through -1.05 V vs. RHE (Figure 5b). The CCE CX_$Sn_{70}Cu_{30}$ produced formate at 190.3 μmol h^{-1} cm^{-2} at -0.89 V, and it remained above 150 μmol h^{-1} cm^{-2} for the same potential range (Figure

5c). The maximum production rate of 199.1 μmol h^{-1} cm^{-2} was achieved with the CCE CX_$Sn_{95}Cu_5$ at -0.72 V vs. RHE, however, it remained above 150 μmol h^{-1} cm^{-2} for a narrow potential range (Figure 5d). Interestingly, the production rate was maximum at the potential of maximum FE for CX_$Sn_{95}Cu_5$ only, and for all other CX_CuO, CX_SnO and CX_$Sn_{70}Cu_{30}$, the maximum production rate was observed at potentials more negative to the potentials of maximum FE.

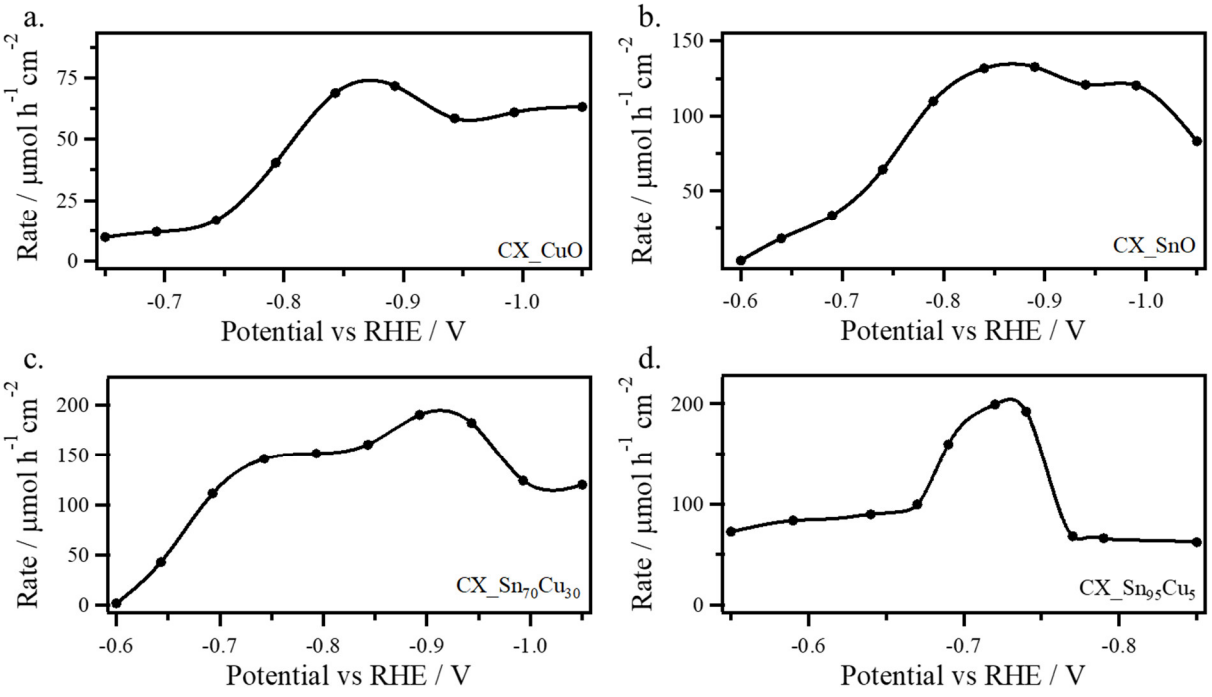

Figure 5. The rates of formate production with different CCEs at the working electrode potentials ranging from -0.55 V to -1.05 V vs. RHE: (a) CX_CuO, (b) CX_SnO, (c) CX_$Sn_{70}Cu_{30}$ and (d) CX_$Sn_{95}Cu_5$. The rates are normalized with the experiment run time and geometric area of electrodes.

The low solubility of CO_2 in aqueous solution leads to mass transfer limitation in the electrochemical conversion of CO_2. Reports reveal that pressurizing the CO_2 feed minimizes mass transfer limitation by increasing the concentration of dissolved CO_2.[43, 59, 71] Here, we slightly increased CO_2 pressure in an H-cell up to 4 psig, using the setup as shown in Figure S10 (Supplementary Information), and carried out the electrochemical reduction of CO_2 to FA in 1 M potassium bicarbonate by using CX_$Sn_{95}Cu_5$. The CCE was charged at -0.74 V vs. RHE, previously determined for optimum performance, and chronoamperometric measurements were

carried out for 4 h at each of the reactor pressures 0, 2, 3.6 and 4.0 psig. Consistent with the results described above (Figure 4d), the CCE showed 69.3% selectivity for formate at -0.74 V vs. RHE at ~0 psig, which increased to 76.5% at 4 psig (Figure 6a). The j in each condition was constant (Figure 6b-d). The slow increase in the j resulting in higher FE accounts for more conversion of CO_2 to FA. This clearly shows that increasing pressure favors the electrochemical reduction of CO_2 to FA by reducing the mass transport limitation.

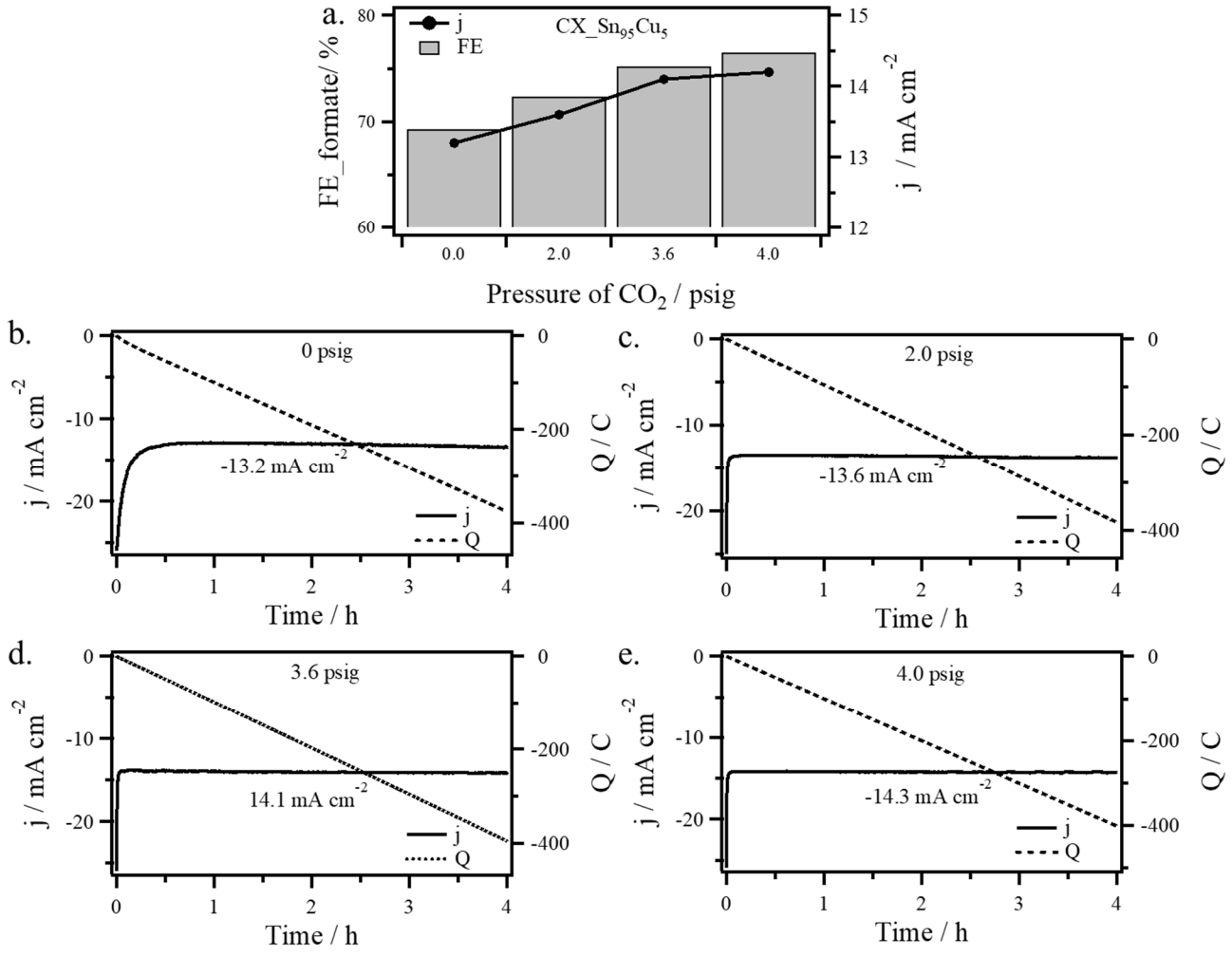

Figure 6. (a) FE for formate and j at -0.74 V vs RHE by using $CX_Sn_{95}Cu_5$ at the pressure of CO_2 ranging from 0 to 4 psig, (b-e) chronoamperometric/coulometric plots at different pressure of CO_2 feed.

For revealing the factors contributing to the observed findings, further research was carried out with cyclic voltammetry and electrochemical impedance spectroscopy in ambient conditions. CX

is not a suitable substrate for these analyses because of its mesoporous structure and high capacitive features resulting in very poor detection of Faradaic features in the cyclic voltammogram. To minimize the interference arising from the capacitive current, CT coated with the $Sn_{95}Cu_5$ (CT_$Sn_{95}Cu_5$) was used as the WE while Pt mesh was the CE. Cyclic voltammetric and electrochemical impedance spectroscopic measurements were carried out using CO_2-saturated potassium bicarbonate solution as a catholyte. First the catholyte solution was purged with dry N_2 gas for 15 min to remove dissolved O_2, and then humidified CO_2 gas was purged for 15 minutes to get a saturated solution of CO_2. Cyclic voltammograms of CT and CT_$Sn_{95}Cu_5$ are shown in Figure 7a. CT sluggishly assists in hydrogen evolution around -0.4 V vs. RHE. Lower j in the CV of CT_$Sn_{95}Cu_5$ in the range of 0 to -0.4 V vs. RHE indicates the catalyst is suppressing HER and a sharp increase in the j thereafter may indicate CO_2 reduction competing with H_2 evolution. Further characterization was performed using electrochemical impedance spectroscopic measurement at the dc potential past -0.4 V vs. RHE. Figures 7b and c depict EIS spectra of the CT_$Sn_{95}Cu_5$ electrode at -0.6 V and -0.7 V vs. RHE. The Nyquist plot (Figure 7b) at -0.7 V shows two semicircles likely corresponding to HER with a time constant in the ms range and another corresponding to CO_2 reduction with a time constant in s (Figure 7c). The corresponding EIS for CT can be found in Figure S11 (Supplementary Information).

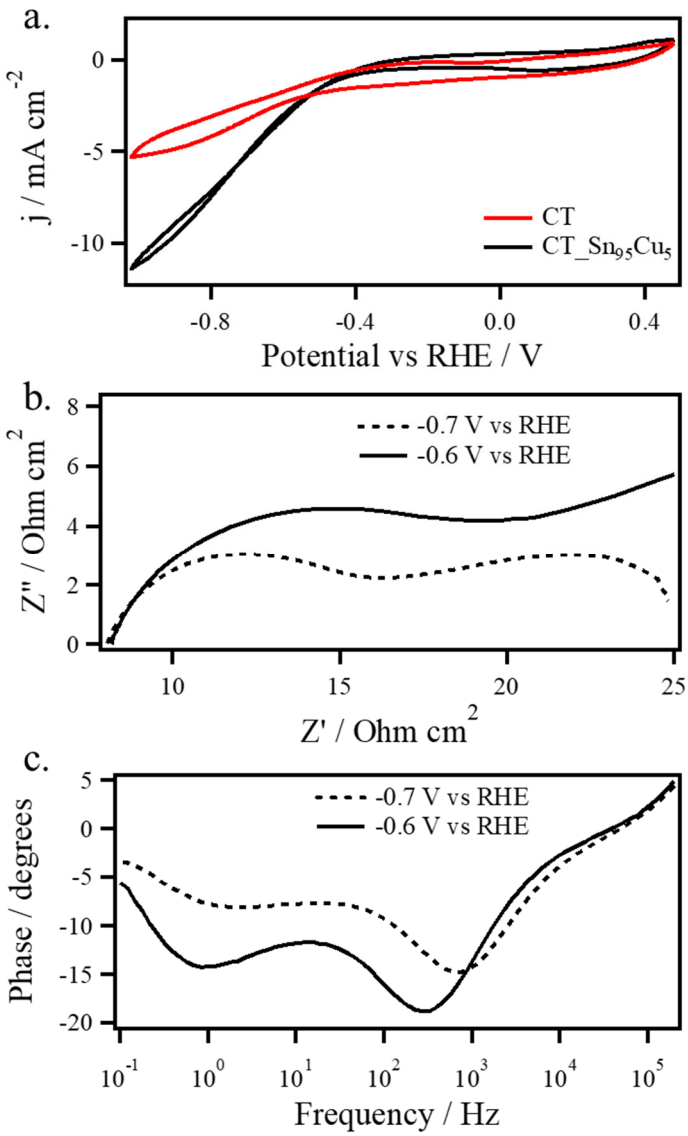

Figure 7. (a) Cyclic voltammetric measurement of the CT and CT_$Sn_{95}Cu_5$ in 50 mM potassium bicarbonate solution. (b) Nyquist plot, and (c) phase plot for the CT_$Sn_{95}Cu_5$. The working electrode potential is expressed vs. RHE after IR correction.

Since aqueous $KHCO_3$ solution, (1) is in equilibrium with dissolved CO_2 and (2) generates CO_2 in the presence of H^+ ions supplied by the BPM as $HCO_3^- + H^+ \rightarrow CO_2 + H_2O$, the features of CO_2 reduction can also be observed without actively purging CO_2 into the catholyte solution. The catholyte solution was purged with dry N_2 gas for 15 min to remove dissolved O_2, and then humidified CO_2 gas was purged for 15 minutes to get a saturated solution of CO_2. It is well known that $KHCO_3$ also acts as an in-situ source of CO_2. However, CO_2 release depends on the $KHCO_3$

concentration, reduction potential, and pH of the electrolyte. Formate production was quantified without actively purging CO_2 into the $KHCO_3$ solution. The chronoamperometric measurements were done at -0.74 V vs. RHE without purging CO_2 gas for at least 3 h for concentrations of $KHCO_3$ ranging from 100 mM through 1 M. Figure 8a shows the FE for formate in $KHCO_3$ solutions and the corresponding rate of formate production. FE increases sharply from 100 mM to 500 mM of potassium bicarbonate, and so does the j (Figures S12 and S13, Supplementary Information). The FE increases more slowly at higher concentrations of $KHCO_3$ (>500 mM). At 1 M $KHCO_3$, 40% of FE comes from $KHCO_3$/along with equilibrium dissolved CO_2. Thus, bicarbonate solution coupled with CO_2 feed provides better electrochemical CO_2RR. Three of these catalysts: SnO, CuO and $Sn_{95}Cu_5$ were tested for their long-term stability using chronoamperometric measurement at the potential for optimal performance as determined before using 0.5 M $KHCO_3$ as a catholyte coupled with bubbling moist CO_2 at 10 mL/min. The chronoamperometric curves for the CCE of these catalysts are depicted in Figure 8b-d. The stable j was observed with CX_CuO for less than 10 h and CX_SnO for less than 30 h. The electrode CX_$Sn_{95}Cu_5$ exhibited good stability for 60 h. Regarding their FE towards formate, the selectivity of CX_CuO and CX_SnO dropped to ~ 50% after 25 h and 60 h of continuous run. The degradation in the performance can be traced to either chemical transformation/poisoning of the catalyst or precipitation of the electrolyte on the active site of the CCE, which appears to be the case here and a focus of ongoing work will be to minimize salt precipitation on the cathode. In the case of CX_$Sn_{95}Cu_5$, the performance was retained within 95% even after 60 h of continuous run. Salt precipitation becomes more prominent with a higher concentration of $KHCO_3$ (>500 mM) and an extended experiment run time. The spent electrodes, namely CX_CuO, CX_SnO, and CX_$Sn_{95}Cu_5$, were examined with scanning electron microscopic imaging, as illustrated in Figure S14 of the Supplementary Information. In a 1 M $KHCO_3$ solution, substantial electrolyte precipitation occurred on the surface even after 25 hours, covering almost the entire surface after 60 hours of continuous operation. It is noteworthy that when utilizing a 0.5 M $KHCO_3$ solution with CO_2 bubbled at the same rate, the precipitation was significantly minimized. The observed performance of CX_$Sn_{95}Cu_5$ can be attributed to the synergistic effect of Sn and Cu, which enhances both stability and selectivity. This effect, combined with reduced mass transfer limitations from a bicarbonate solution of suitable concentration coupled with CO_2, accounts for the observed performance of CX_$Sn_{95}Cu_5$.

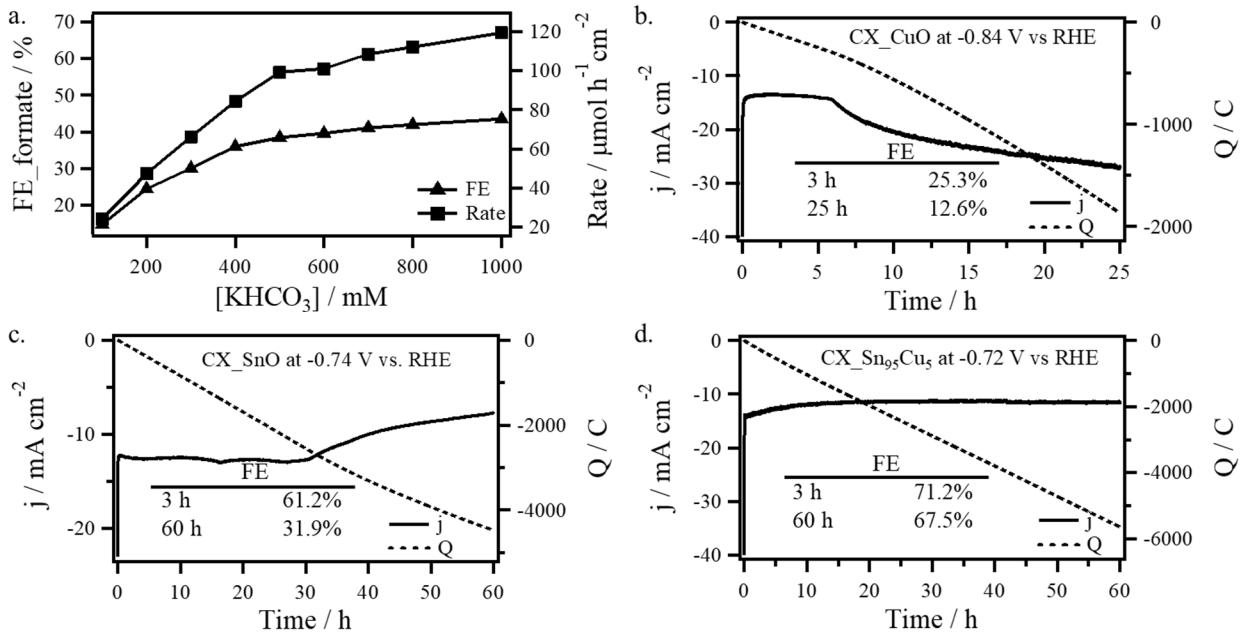

Figure 8. (a) FE and rate of formate production with CX_$Sn_{95}Cu_5$ in $KHCO_3$ solutions with concentrations from 100 mM through 1000 mM at -0.74 V vs. RHE, and (b-d) chronoamperometric/coulometric plots for CX_CuO, CX_SnO and CX_$Sn_{95}Cu_5$ for long-term testing.

Most reports using SnCu catalysts for electrochemical reduction of CO_2 were carried out in flow through reactors using cation/anion exchange membranes or no membrane and combinations of $NaHCO_3$/KOH, KOH/$KHCO_3$, $KHCO_3$/$KHCO_3$ and KOH/KOH as catholytes/anolytes yielding good current densities (18-225 mA cm^{-2}) and FEs (80-90%). The work shown here used an H-cell with a bipolar membrane separating 0.5 M $KHCO_3$ (catholyte) and (0.4 M anolyte) making direct comparisons difficult. The comparative current densities and FEs were somewhat higher than what was obtained with the H-cell (15.6 mA cm^{-2}, 71.2%). These differences are likely because H-cells generally suffer from a large mass transfer limitation, and also huge potential drop due to large distance between the cathode and anode and pH gradient across the BPM as mentioned by Ramdin et al. and others.[56, 59, 72, 73] But by minimizing mass transfer limitations through increasing the pressure of CO_2 feed to 4 psig, we were able to achieve FE of 76.5% for formate production, closely aligning with previous observations, even with the limitations of the H-cell. However, it's worth noting that this was accomplished at a lower potential

of -0.74 V vs. RHE, compared to the -1 V vs. RHE or higher potentials reported in earlier studies.[56, 72] Moreover, our simple H-cell electrochemical reactor employing the SnCu catalyst demonstrated impressive stability, continuously producing formate at a uniform rate for over 60 hours, in contrast to the 42-hour stability reported in prior research.[72] Additionally, this report presents the reports on spent electrodes, providing further insights into minimization of electrolyte precipitation to retain the performance of the electrochemical reactor.

Conclusions

Synergistic bimetallic electrocatalysts can improve the activity and selectivity over their monometallic counterparts by tuning the structure, morphology, and composition. In the electrochemical reduction of CO_2, the adsorption and orientation of $CO_2^{\cdot-}$ are changed by the synergistic effect, thereby creating varieties of reduction products. Bimetallic SnCu oxides with 100, 95, 70 and 0 mol% of Sn were synthesized and tested for CO_2 reduction to FA. Incorporating Cu into SnO increased the selectivity for FA production with a wider potential window and reduced overpotential. Most importantly, suppressing the parasitic competing reactions, the selectivity of SnCu oxide remained stabilized within 95% of the initial value even after 60 h of continuous run. Under identical conditions, the performance of SnO and CuO dropped to 50% in ~7 h and ~ 30 h, respectively. We also showed that FA can be formed in an actively-purged or non-purged system. Our results with best performing SnCu oxide reveal that the contribution from bicarbonate solution ranges from ~ 15% to 40% when the concentration of bicarbonate solution ranges from 100 mM solution to ~40% in 1 M bicarbonate solution without purging CO_2. Finally, the conversion of CO_2 to FA was further boosted by ~ 7% on increasing the pressure of CO_2 feed to 4 psig. In the case of CX_$Sn_{95}Cu_5$, the performance was retained within 95% even after 60 h of continuous run. Our lab-scale electrochemical cell with SnCu oxide supported on the mesoporous carbon xerogel enhances the CO_2 solubility, minimizes the precipitation of salts that can degrade the performance, and suppresses the competitive hydrogen evolution reaction, demonstrating the feasibility of using our catalyst and system for the electrochemical conversion of CO_2 into formic acid with high selectivity, productivity, and stability. This could have significant implications for the mitigation of CO_2 emissions and the development of sustainable chemical industry.

Associated Content

Supplementary data associated with this article can be found in the online version at …. and includes the following: Temperature ramp of the furnace during the synthesis of carbon xerogel, Digital picture of actual electrochemical cell, Scanning electron microscopic images of commercial carbon cloth and carbon xerogel, Four-probe method for solid-state conductivity measurement, Solid-state conductivity of commercial carbon and carbon xerogel, energy dispersive X-ray spectra of as synthesized SnCu oxides, X-ray diffraction spectra of commercial Cu_2O and CuO, Chronoamperometric/coulometric curves for CX_CuO, CX_SnO, CX_$Sn_{70}Cu_{30}$ and CX_$Sn_{95}Cu_5$ at the potentials where FA was produced significantly, Experimental setup for increasing the pressure of CO_2 feed in an H-Cell, Electrochemical impedance spectra of CeTech carbon cloth, Chronoamperometric/coulometric plots for the CCEs CX_$Sn_{95}Cu_5$ in $KHCO_3$ solutions of concentrations ranging from 100 mM through 1000 mM at -0.74 V, and Analysis of the spent electrodes from the electrochemical reduction of CO_2 under different conditions.

Author Information

Corresponding Author

Email: jesse.thompson@uky.edu (Jesse Thompson)

Author Contributions

Pom L. Kharel: writing, investigation, visualization, formal analysis; **Muthu K. Gnanamani**: catalyst synthesis; **Md Ariful Hoque** and **Keemia Abad**: investigation, formal analysis; **Neng Huang** and **Xin Gao**: characterization and synthesis; **Kunlei Liu**: funding acquisition, project administration, supervision; **Ayokunle O. Omosebi**: funding acquisition, conceptualization, visualization, supervision, review, editing, validation; **Jesse Thompson**: funding acquisition, conceptualization, supervision, review, editing, project administration, resources.

Declaration of Competing Interest

The authors declare that they have no known competing financial interests or personal relationships that could have appeared to influence the work reported in this paper.

Acknowledgment

This material is based upon work supported by the Department of Energy under Award Number DE-FE0031920.

Abbreviations

CE: counter electrode

CO_2RR: CO_2 reduction reaction

CT: CeTech carbon cloth

CV: cyclic voltammetry

CX: carbon xerogel

FA: formic acid

FE: faradaic efficiency

HER: hydrogen evolution reaction

RE: reference electrode

RHE: reversible hydrogen electrode

WE: working electrode

References

(1) https://climate.nasa.gov/vital-signs/carbon-dioxide/ (accessed 2024 January 19).
(2) Welch, A. J.; Dunn, E.; DuChene, J. S.; Atwater, H. A. Bicarbonate or carbonate processes for coupling carbon dioxide capture and electrochemical conversion. *ACS Ener. Lett.* **2020**, *5*, 940-945.

(3) Xia, W.; Ren, Y.-Y.; Liu, J.; Deng, B.-Y.; Wang, F. Non-synergistic photocatalysis of CO_2-to-CO conversion by a binuclear complex of rigidly linking two cobalt catalytic centers. *J. Photochem. Photobiol., A* **2022**, *426*, 113754.
(4) Liu, X.; Zhong, H.; Wang, C.; He, D.; Jin, F. CO_2 reduction into formic acid under hydrothermal conditions: A mini review. *Energy Sci. Eng.* **2022**, *10*, 1601-1613.
(5) Quintana-Gómez, L.; Martínez-Álvarez, P.; Segovia, J. J.; Martín, Á.; Bermejo, M. D. Hydrothermal reduction of CO_2 captured as $NaHCO_3$ into formate with metal reductants and catalysts. *J. CO_2 Util.* **2023**, *68*, 102369.
(6) Lodh, J.; Roy, S. Bio-inspired CO_2 reduction reaction catalysis using soft-oxometalates. *J. Inorg. Biochem.* **2022**, 111903.
(7) Yadav, V.; Purkait, M. Solar cell driven electrochemical process for the reduction of CO_2 to HCOOH on Zn and Sn electrocatalysts. *Sol. Energy* **2016**, *124*, 177-183.
(8) Yoo, J. S.; Christensen, R.; Vegge, T.; Nørskov, J. K.; Studt, F. Theoretical insight into the trends that guide the electrochemical reduction of carbon dioxide to formic acid. *ChemSusChem* **2016**, *9*, 358-363.
(9) Lv, W.; Zhang, R.; Gao, P.; Lei, L. Studies on the faradaic efficiency for electrochemical reduction of carbon dioxide to formate on tin electrode. *J. Power Sources* **2014**, *253*, 276-281.
(10) Hori, Y. CO_2-Reduction, Catalyzed by metal electrodes. *Handbook of Fuel Cells* **2010**.
(11) Kortlever, R.; Shen, J.; Schouten, K. J. P.; Calle-Vallejo, F.; Koper, M. T. Catalysts and reaction pathways for the electrochemical reduction of carbon dioxide. *J. Phys. Chem. Lett.* **2015**, *6*, 4073-4082.
(12) Lu, X.; Leung, D. Y.; Wang, H.; Leung, M. K.; Xuan, J. Electrochemical reduction of carbon dioxide to formic acid. *ChemElectroChem* **2014**, *1*, 836-849.
(13) Feaster, J. T.; Shi, C.; Cave, E. R.; Hatsukade, T.; Abram, D. N.; Kuhl, K. P.; Hahn, C.; Nørskov, J. K.; Jaramillo, T. F. Understanding selectivity for the electrochemical reduction of carbon dioxide to formic acid and carbon monoxide on metal electrodes. *ACS Catal.* **2017**, *7*, 4822-4827.
(14) Liang, S.; Altaf, N.; Huang, L.; Gao, Y.; Wang, Q. Electrolytic cell design for electrochemical CO_2 reduction. *J. CO_2 Util.* **2020**, *35*, 90-105.
(15) Zheng, X.; De Luna, P.; de Arquer, F. P. G.; Zhang, B.; Becknell, N.; Ross, M. B.; Li, Y.; Banis, M. N.; Li, Y.; Liu, M. Sulfur-modulated tin sites enable highly selective electrochemical reduction of CO_2 to formate. *Joule* **2017**, *1*, 794-805.
(16) Moreno, D.; Omosebi, A.; Jeon, B. W.; Abad, K.; Kim, Y. H.; Thompson, J.; Liu, K. Electrochemical CO_2 conversion to formic acid using engineered enzymatic catalysts in a batch reactor. *J. CO_2 Util.* **2023**, *70*, 102441.
(17) Ewis, D.; Arsalan, M.; Khaled, M.; Pant, D.; Ba-Abbad, M. M.; Amhamed, A.; El-Naas, M. H. Electrochemical reduction of CO2 into formate/formic acid: A review of cell design and operation. *Sep. Purif. Technol.* **2023**, 123811.
(18) Zhao, R.; Ding, P.; Wei, P.; Zhang, L.; Liu, Q.; Luo, Y.; Li, T.; Lu, S.; Shi, X.; Gao, S. Recent progress in electrocatalytic methanation of CO_2 at ambient conditions. *Adv. Funct. Mater.* **2021**, *31*, 2009449.
(19) Duarah, P.; Haldar, D.; Yadav, V.; Purkait, M. K. Progress in the electrochemical reduction of CO_2 to formic acid: A review on current trends and future prospects. *J. Environ. Chem. Eng.* **2021**, *9*, 106394.
(20) Boutin, E.; Robert, M. Molecular electrochemical reduction of CO_2 beyond two electrons. *Trends Chem.* **2021**, *3*, 359-372.

(21) Wissink, T.; van de Poll, R. C.; Figueiredo, M. C.; Hensen, E. J. Stability of In_2O_3 nanoparticles in PTFE-containing gas diffusion electrodes for CO_2 electroreduction to formate. *Appl. Surf. Sci.* **2023**, *67*, 102331.
(22) Kim, S.; Dong, W. J.; Gim, S.; Sohn, W.; Park, J. Y.; Yoo, C. J.; Jang, H. W.; Lee, J.-L. Shape-controlled bismuth nanoflakes as highly selective catalysts for electrochemical carbon dioxide reduction to formate. *Nano Energy* **2017**, *39*, 44-52.
(23) Zhang, Q.; Du, J.; He, A.; Liu, Z.; Tao, C. Low overpotential electrochemical CO_2 reduction to formate on Co_3O_4–CeO_2/low graphitic carbon catalyst with oxygen vacancies. *J. Solid State Chem.* **2019**, *279*, 120946.
(24) Huan, T. N.; Simon, P.; Benayad, A.; Guetaz, L.; Artero, V.; Fontecave, M. Cu/Cu_2O electrodes and CO_2 reduction to formic acid: Effects of organic additives on surface morphology and activity. *Chem. Eur. J.* **2016**, *22*, 14029-14035.
(25) Luo, W.; Xie, W.; Mutschler, R.; Oveisi, E.; De Gregorio, G. L.; Buonsanti, R.; Züttel, A. Selective and stable electroreduction of CO_2 to CO at the copper/indium interface. *ACS Catal.* **2018**, *8*, 6571-6581.
(26) Aksu, T.; Baytok, E.; Karslı, M. A.; Muruz, H. Effects of formic acid, molasses and inoculant additives on corn silage composition, organic matter digestibility and microbial protein synthesis in sheep. *Small Rumin. Res.* **2006**, *61*, 29-33.
(27) Wang, W.-H.; Himeda, Y.; Muckerman, J. T.; Manbeck, G. F.; Fujita, E. CO_2 hydrogenation to formate and methanol as an alternative to photo-and electrochemical CO_2 reduction. *Chem. Rev.* **2015**, *115*, 12936-12973.
(28) Aresta, M.; Dibenedetto, A.; Angelini, A. Catalysis for the valorization of exhaust carbon: from CO_2 to chemicals, materials, and fuels. Technological use of CO_2. *Chem. Rev.* **2014**, *114*, 1709-1742.
(29) Philips, M. F.; Gruter, G.-J. M.; Koper, M. T.; Schouten, K. J. P. Optimizing the electrochemical reduction of CO_2 to formate: a state-of-the-art analysis. *ACS Sustain. Chem. Eng.* **2020**, *8*, 15430-15444.
(30) Proietto, F.; Patel, U.; Galia, A.; Scialdone, O. Electrochemical conversion of CO_2 to formic acid using a Sn based electrode: a critical review on the state-of-the-art technologies and their potential. *Electrochim. Acta* **2021**, *389*, 138753.
(31) Ma, Z.; Legrand, U.; Pahija, E.; Tavares, J. R.; Boffito, D. C. From CO_2 to formic acid fuel cells. *Ind. Eng. Chem. Res.* **2020**, *60*, 803-815.
(32) Deng, P.; Wang, H.; Qi, R.; Zhu, J.; Chen, S.; Yang, F.; Zhou, L.; Qi, K.; Liu, H.; Xia, B. Y. Bismuth oxides with enhanced bismuth–oxygen structure for efficient electrochemical reduction of carbon dioxide to formate. *ACS Catal.* **2019**, *10*, 743-750.
(33) Lee, J.; Liu, H.; Chen, Y.; Li, W. Bismuth nanosheets derived by in situ morphology transformation of bismuth oxides for selective electrochemical CO_2 reduction to formate. *ACS Appl. Mater. Interfaces* **2022**, *14*, 14210-14217.
(34) Jiang, X.; Lin, L.; Rong, Y.; Li, R.; Jiang, Q.; Yang, Y.; Gao, D. Boosting CO_2 electroreduction to formate via bismuth oxide clusters. *Nano Res.* **2023**, *16*, 12050-12057.
(35) Agarwal, A. S.; Zhai, Y.; Hill, D.; Sridhar, N. The electrochemical reduction of carbon dioxide to formate/formic acid: engineering and economic feasibility. *ChemSusChem* **2011**, *4*, 1301-1310.
(36) Chen, Y.; Kanan, M. W. Tin oxide dependence of the CO_2 reduction efficiency on tin electrodes and enhanced activity for tin/tin oxide thin-film catalysts. *J. Am. Chem. Soc.* **2012**, *134*, 1986-1989.

(37) Zhao, S.; Li, S.; Guo, T.; Zhang, S.; Wang, J.; Wu, Y.; Chen, Y. Advances in Sn-based catalysts for electrochemical CO 2 reduction. *Nano-Micro Lett.* **2019**, *11*, 1-19.
(38) Zhang, Y.; Li, Z.; Jang, H.; Wei, X.; Qin, Q.; Liu, X. Electrochemical conversion of CO_2 into $HCOO^-$ in a synergistic manner by a nanocomposite of Zn_2SnO_4/ZnO. *Inorg. Chem. Fron.* **2023**, *10*, 1818-1825.
(39) Bhalothia, D.; Liu, H.-Y.; Chen, S.-H.; Tseng, Y.-T.; Li, W.; Dai, S.; Wang, K.-W.; Chen, T.-Y. The sub-nanometer In_2O clusters on Ag nanoparticles with highly selective electrochemical CO_2 reduction to formate. *Chem. Eng. J.* **2024**, *481*, 148295.
(40) Lee, W.; Kim, Y. E.; Youn, M. H.; Jeong, S. K.; Park, K. T. Catholyte-free electrocatalytic CO_2 reduction to formate. *Angew. Chem. Int. Ed.* **2018**, *57*, 6883-6887.
(41) Yang, H.; Kaczur, J. J.; Sajjad, S. D.; Masel, R. I. Electrochemical conversion of CO_2 to formic acid utilizing Sustainion™ membranes. *J. of CO_2 Util.* **2017**, 208-217.
(42) Chen, Y.; Vise, A.; Klein, W.; Cetinbas, F.; Myers, D.; Smith, W.; Deutsch, T.; Neyerlin, K. Scalable platform for the electrochemical conversion of CO2 to formate: identifying pathways to higher energy efficiencies. ACS Energy Lett.; Vol. 5, pp 1825-1833.
(43) Li, J.; Kuang, Y.; Meng, Y.; Tian, X.; Hung, W.-H.; Zhang, X.; Li, A.; Xu, M.; Zhou, W.; Ku, C.-S. Electroreduction of CO_2 to formate on a copper-based electrocatalyst at high pressures with high energy conversion efficiency. *J. Am. Chem. Soc.* **2020**, *142*, 7276-7282.
(44) Zheng, T.; Liu, C.; Guo, C.; Zhang, M.; Li, X.; Jiang, Q.; Xue, W.; Li, H.; Li, A.; Pao, C.-W. Copper-catalysed exclusive CO_2 to pure formic acid conversion via single-atom alloying. *Nature Nanotechnol.* **2021**, *16*, 1386-1393.
(45) Yin, Z.; Gao, D.; Yao, S.; Zhao, B.; Cai, F.; Lin, L.; Tang, P.; Zhai, P.; Wang, G.; Ma, D. Highly selective palladium-copper bimetallic electrocatalysts for the electrochemical reduction of CO_2 to CO. *Nano Energy* **2016**, 35-43.
(46) Wang, M.; Liu, S.; Chen, B.; Tian, F.; Peng, C. Synergistic geometric and electronic effects in Bi–Cu bimetallic catalysts for CO_2 electroreduction to formate over a wide potential window. *ACS Sustain. Chem. Eng.* **2022**, *10*, 5693-5701.
(47) Azenha, C.; Mateos-Pedrero, C.; Lagarteira, T.; Mendes, A. M. Tuning the selectivity of Cu_2O/ZnO catalyst for CO_2 electrochemical reduction. *J. CO_2 Util.* **2023**, *68*, 102368.
(48) Wang, Q.; Yang, X.; Zang, H.; Liu, C.; Wang, J.; Yu, N.; Kuai, L.; Qin, Q.; Geng, B. InBi bimetallic sites for efficient electrochemical reduction of CO_2 to HCOOH. *Small* **2023**, *19*, 2303172.
(49) Wang, C.; He, A.; Zhang, N.; Sui, H.; Wen, Z.; Xu, C.; Yan, G.; Xue, R. Zn-Bi bimetallic catalyst for electrochemical synthesis of C1 products by highly selective CO_2 reduction. *J. Catal.* **2023**, *428*, 115128.
(50) Sarfraz, S.; Garcia-Esparza, A. T.; Jedidi, A.; Cavallo, L.; Takanabe, K. Cu–Sn bimetallic catalyst for selective aqueous electroreduction of CO_2 to CO. *ACS Catal.* **2016**, *6*, 2842-2851.
(51) Yan, J.; Guan, Y.; Marchetti, B.; Liu, Y.; Ning, F.; Yi, J.; Zhou, X.-D. Bi-Eu bimetallic catalysts enabling ultrastable electroreduction of CO_2 with a ~ 100% formate faradaic efficiency. *Chem. Eng. J.* **2023**, *467*, 143531.
(52) Liu, W.; Ding, L.; Liu, M.; Wang, X.; Zhang, Z.; Jiang, T.-W.; Huo, S.; Cai, W.-B. Unraveling the interfacial effect of PdBi bimetallic catalysts on promoting CO_2 electroreduction to formate. *Nano Res.* **2023**, 1-10.
(53) Yang, C.; Hu, Y.; Li, S.; Huang, Q.; Peng, J. Self-supporting Bi–Sb bimetallic nanoleaf for electrochemical synthesis of formate by highly selective CO_2 reduction. *ACS Appl. Mater. Interfaces* **2023**, *15*, 6942-6950.

(54) Chang, S.; Xuan, Y.; Wang, Q.; Wang, K. Bimetallic In–Sn core–shell catalyst enabling highly efficient electrocatalytic CO_2 reduction to formate. *ACS Appl. Eng. Mater.* **2023**, *1*, 1514-1523.
(55) Liu, W.; Zhang, Z.; Huo, S.; Ren, Q.; Liu, M. Bimetallic Zn_3Sn_2 electrocatalyst derived from mixed oxides enhances formate production towards CO_2 electroreduction reaction. *Appl. Surf. Sci.* **2023**, *608*, 155110.
(56) Liu, P.-X.; Peng, L.-W.; He, R.-N.; Li, L.-L.; Qiao, J.-L. A high-performance continuous-flow MEA reactor for electroreduction CO_2 to formate. *J. Electrochem.* **2022**, *28*, 2104231.
(57) Landon, J.; Gao, X.; Kulengowski, B.; Neathery, J. K.; Liu, K. Impact of pore size characteristics on the electrosorption capacity of carbon xerogel electrodes for capacitive deionization. *J. Electrochem. Soc.* **2012**, *159*, A1861.
(58) Jaśkaniec, S.; Kavanagh, S. R.; Coelho, J.; Ryan, S.; Hobbs, C.; Walsh, A.; Scanlon, D. O.; Nicolosi, V. Solvent engineered synthesis of layered SnO for high-performance anodes. *NPJ 2D Mater. Appl.* **2021**, *5*, 1-9.
(59) Ramdin, M.; Morrison, A. R.; De Groen, M.; Van Haperen, R.; De Kler, R.; Van Den Broeke, L. J.; Trusler, J. M.; De Jong, W.; Vlugt, T. J. High pressure electrochemical reduction of CO_2 to formic acid/formate: a comparison between bipolar membranes and cation exchange membranes. *Ind. Eng. Chem. Res.* **2019**, *58*, 1834-1847.
(60) Hwang, U.-S.; Choi, J.-H. Changes in the electrochemical characteristics of a bipolar membrane immersed in high concentration of alkaline solutions. *Sep. Purif. Technol.* **2006**, *48*, 16-23.
(61) Abdi, F. F.; van de Krol, R. Nature and light dependence of bulk recombination in Co-Pi-catalyzed $BiVO_4$ photoanodes. *J. Phy. Chem. C* **2012**, *116*, 9398-9404.
(62) Jouhannaud, J.; Rossignol, J.; Stuerga, D. Rapid synthesis of tin (IV) oxide nanoparticles by microwave induced thermohydrolysis. *J. Solid State Chem.* **2008**, *181*, 1439-1444.
(63) Patil, G. E.; Kajale, D. D.; Gaikwad, V. B.; Jain, G. H. Preparation and characterization of SnO_2 nanoparticles by hydrothermal route. *Int. Nano Lett.* **2012**, *2*.
(64) Janardhan, E.; Reddy, M. M.; Reddy, P. V.; Reddy, M. J. Synthesis of SnO nanopatricles—a hydrothermal approach. *W. J. Nano Sci. Eng.* **2018**, *8*, 33-37.
(65) Jo, Y. H.; Park, J. C.; Bang, J. U.; Song, H.; Lee, H. M. New synthesis approach for low temperature bimetallic nanoparticles: size and composition controlled Sn–Cu nanoparticles. *J. Nanosci. Nanotechnol.* **2011**, *11*, 1037-1041.
(66) Yang, D.; Zhu, Q.; Chen, C.; Liu, H.; Liu, Z.; Zhao, Z.; Zhang, X.; Liu, S.; Han, B. Selective electroreduction of carbon dioxide to methanol on copper selenide nanocatalysts. *Nat. Commun.* **2019**, *10*, 677.
(67) Tan, D.; Lee, W.; Park, K. T.; Jeon, Y. E.; Hong, J.; Ko, Y. N.; Kim, Y. E. Promoting CO_2 reduction to formate selectivity on indium-doped tin oxide nanowires. *Appl. Surf. Sci.* **2023**, *613*, 155944.
(68) Oßkopp, M.; Löwe, A.; Lobo, C. M.; Baranyai, S.; Khoza, T.; Auinger, M.; Klemm, E. Producing formic acid at low pH values by electrochemical CO_2 reduction. *J. CO_2 Util.* **2022**, *56*, 101823.
(69) Abdinejad, M.; Khorasani-Motlagh, M.; Noroozifar, M.; Kraatz, H.-B. Electroreduction of carbon dioxide to formate using highly efficient bimetallic Sn-Pd aerogels. *Mater. Adv.* **2022**, *3*, 1224-1230.

(70) Zou, J.; Lee, C. Y.; Wallace, G. G. Boosting formate production from CO_2 at high current densities over a wide electrochemical potential window on a SnS catalyst. *Adv. Sci.* **2021**, *8*, 2004521.
(71) Wang, L.; Nitopi, S. A.; Bertheussen, E.; Orazov, M.; Morales-Guio, C. G.; Liu, X.; Higgins, D. C.; Chan, K.; Nørskov, J. K.; Hahn, C. Electrochemical carbon monoxide reduction on polycrystalline copper: Effects of potential, pressure, and pH on selectivity toward multicarbon and oxygenated products. *ACS Catal.* **2018**, *8*, 7445-7454.
(72) Wang, J.; Zou, J.; Hu, X.; Ning, S.; Wang, X.; Kang, X.; Chen, S. Heterostructured intermetallic CuSn catalysts: high performance towards the electrochemical reduction of CO_2 to formate. *J. Mater. Chem. A* **2019**, *7*, 27514-27521.
(73) Wang, W.; Wang, Z.; Yang, R.; Duan, J.; Liu, Y.; Nie, A.; Li, H.; Xia, B. Y.; Zhai, T. In situ phase separation into coupled interfaces for promoting CO_2 electroreduction to formate over a wide potential window. *Angew. Chem. Int. Ed.* **2021**, *60*, 22940-22947.